Electronic Quenching of OH A 2 Σ + Induced by Collisions with Kr Atoms

ARTICLE *in* THE JOURNAL OF PHYSICAL CHEMISTRY A · AUGUST 2013

Impact Factor: 2.69 · DOI: 10.1021/jp407035p · Source: PubMed

THE JOURNAL OF PHYSICAL CHEMISTRY A

Article

pubs.acs.org/JPCA

Electronic Quenching of OH A $^2\Sigma^+$ Induced by Collisions with Kr Atoms

Julia H. Lehman,[†] Marsha I. Lester,*[,†] Jacek Kłos,[‡] Millard H. Alexander,[‡,§] Paul J. Dagdigian,[∥] Diego Herráez-Aguilar,[⊥] F. Javier Aoiz,[⊥] Mark Brouard,[#] Helen Chadwick,[#] Tom Perkins,[#] and Scott A. Seamons[#]

[†]Department of Chemistry, University of Pennsylvania, Philadelphia, Pennsylvania 19104-6323, United States

[‡]Department of Chemistry and Biochemistry and [§]Institute for Physical Science and Technology, University of Maryland, College Park, Maryland 20742-2021, United States

[∥]Department of Chemistry, The Johns Hopkins University, Baltimore, Maryland 21218-2685, United States

[⊥]Departamento de Quimica Fisica, Facultad de Quimica, Universidad Complutense, Madrid 28040, Spain

[#]The Physical and Theoretical Chemistry Laboratory, Department of Chemistry, University of Oxford, South Parks Road, Oxford OX1 3QZ, United Kingdom

ABSTRACT: Electronic quenching of OH A $^2\Sigma^+$ by Kr was investigated through experimental studies of the collision cross sections and the OH X $^2\Pi$ product state distribution. The quenching cross sections decrease with increasing rotational excitation in the excited OH A $^2\Sigma^+$ electronic state. The OH X $^2\Pi$ products of quenching exhibit a significant degree of rotational excitation but minimal vibrational excitation. Complementary theoretical studies of the OH (A $^2\Sigma^+$, X $^2\Pi$) + Kr potential energy surfaces (PESs), nonadiabatic coupling, and quasiclassical trajectory calculations were carried out to elucidate the quenching dynamics. Accurate PESs for the two lowest diabatic states of A′ symmetry were computed along with the angularly dependent coupling between them. Coupling in nearly linear HO−Kr configurations provides the mechanism for the observed electronic quenching. A deep attractive well on the OH A $^2\Sigma^+$ + Kr PES facilitates access to this region of strong coupling. Surface-hopping quasiclassical trajectory calculations yielded quenching cross sections and a OH X $^2\Pi$ product rotational distribution in good accord with experimental observations.

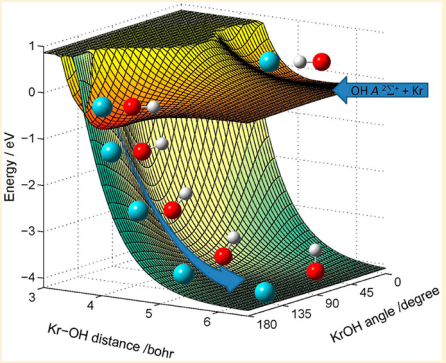

INTRODUCTION

The hydroxyl radical is an important species in atmospheric and combustion environments, often detected using laser-induced fluorescence (LIF) on the OH A $^2\Sigma^+$–X $^2\Pi$ band system.[1] However, extensive kinetics studies have shown that these radicals are efficiently removed from the excited A $^2\Sigma^+$ state via collisions with molecular or atomic partners, resulting in dramatically reduced fluorescence lifetimes and quantum yields. Kinetics studies carried out over a variety of temperatures and initial OH A $^2\Sigma^+$ rotational levels have shown that the rates decrease with increasing temperature and OH A $^2\Sigma^+$ rotational excitation.[2−5] A recent example of such studies is the quenching cross section measurements for various spin−rotation levels of OH A $^2\Sigma^+$ for Kr by Chadwick et al.[6] These trends are indicative of a quenching mechanism controlled by an attractive interaction on the excited state potential energy surface (PES) that depends on the OH orientation.[2−5]

Molecular partners, such as H_2 (~8 Å^2) and N_2 (~5 Å^2), have large quenching cross sections at room temperature. On the other hand, light rare gas colliders typically have negligibly small quenching cross sections ($\sigma_Q \approx 0.004$ and 0.047 Å^2 for He and Ar, respectively).[7−9] In contrast, the heavier rare gases, starting with Kr ($\sigma_Q \approx 8$ Å^2 at 300 K),[6] have quenching cross sections very similar in magnitude to those of the molecular partners.[10] As we show in this study, the PESs emanating from the OH A $^2\Sigma^+$ and X $^2\Pi$ states cross at energies thermally accessible from the excited state.

To gain further insight into the quenching mechanism, recent experimental studies in one of our laboratories (University of Pennsylvania), and others,[11,12] have focused on the outcomes of the quenching event. The characteristics of reactive events (forming new products) and/or nonreactive events (returning OH to its ground X $^2\Pi$ state) have been studied for several quenching partners (H_2, D_2, N_2, CO, CO_2, O_2).[11,13−20] Branching fractions have also been determined.[14−20] The importance of the nonreactive OH X $^2\Pi$ (v'' = 0−2) pathways varies significantly with collision partner, ranging, for example, from 12% for H_2 to ≥ 88% for N_2. The Oxford laboratory has focused on the fate of the electronically

Special Issue: Terry A. Miller Festschrift

Received: July 16, 2013
Revised: August 20, 2013
Published: August 21, 2013

   dx.doi.org/10.1021/jp407035p | J. Phys. Chem. A 2013, 117, 13481−13490

excited OH that survives the quenching process and remains electronically excited after the collision.

On the other hand, the characteristics of the OH X $^2\Pi$ product state distributions following nonreactive quenching of OH A $^2\Sigma^+$, in which 4.06 eV of electronic energy is released to the products, are quite similar for most collision partners. The OH X $^2\Pi$ product is released with a high degree of rotational excitation but little vibrational excitation. In the OH + H_2 system, the rotational distribution is peaked about $N'' = 15$ with an average rotational energy $\langle E_{rot} \rangle = 4480$ cm^{-1} in $v'' = 0$. OH X $^2\Pi$ is produced predominately in $v'' = 0$ (75%), with fewer products found in $v'' = 1$ (20%) and $v'' = 2$ (5%). Collisional quenching with N_2 results in an even higher degree of rotation ($\langle E_{rot} \rangle = 6540$ cm^{-1} in $v'' = 0$), with less energy going into OH vibration (97% of the products are found in $v'' = 0$). Both collision partners also show a preference for populating the $\Pi(A')$ Λ-doublet component, where the unpaired electron of OH X $^2\Pi$ lies in a pπ orbital within the plane of nuclear rotation.[21] For collisions of OH A $^2\Sigma^+$ with Kr, only nonreactive quenching can occur. On the basis of the OH X $^2\Pi$ product state distributions seen in other systems, we might anticipate similar trends following quenching by Kr.

The pairing of experiment with theory has been essential for understanding the quenching process. For this reason, the OH + H_2 system has emerged as a benchmark for elucidating the quenching mechanism. Theoretical work has identified regions of conical intersection accessible from OH A $^2\Sigma^+$ + H_2 when the oxygen side of OH points toward H_2.[13,22−25] These regions of strong nonadiabatic coupling allow population to be funneled from the excited-state surface to OH X $^2\Pi$ + H_2 or H_2O + H products. Interestingly, when the hydrogen side of OH A $^2\Sigma^+$ points toward H_2, there is an attractive electrostatic interaction but no pathway leading to quenching.[13,23,26]

Characteristics of the conical intersection and topography of the PES have been used to explain, at least qualitatively, the significant rotational and minimal vibrational excitation of the OH X $^2\Pi$ products.[13,22,25] Recently, classical trajectory[19,27−29] and quantum scattering calculations[30,31] for the OH A $^2\Sigma^+$ + H_2 system yielded OH X $^2\Pi$ product distributions and branching fractions similar to those measured experimentally. In the OH + N_2 system, ab initio calculations identified an energetically accessible conical intersection coupling the ground and electronically excited state surfaces, again when the oxygen side of OH A $^2\Sigma^+$ points toward the N_2 partner.[17] In the OH−N_2 configuration, there is also an attractive intermolecular interaction but no pathway for quenching.[23] The forces in the region of conical intersection indicate a propensity toward nonreactive products with a large degree of OH rotation and comparatively less OH vibration with N_2 than predicted for H_2, which is consistent with experimental results.[17]

The majority of previous experimental and theoretical studies for the OH (X $^2\Pi$, A $^2\Sigma^+$) + Kr system have been focused on the OH−Kr van der Waals complex formed when the H side of OH X $^2\Pi$ interacts with Kr and its subsequent electronic excitation.[32−35] High-resolution electronic spectroscopy studies by Miller and co-workers enabled the analysis of several vibronic bands of OH−Kr on the OH A $^2\Sigma^+$−X $^2\Pi$ transition.[32,33] These authors derived rotational constants and bond lengths for the ground state and several vibronic levels in the excited electronic state. In addition, they characterized intermolecular stretch progressions with and without bend excitation in the excited electronic state. The spectroscopic data were then utilized to develop an empirical PES for OH A $^2\Sigma^+$ + Kr that was reliable primarily in the $\theta \leq 60°$ region about the linear OH−Kr (Jacobi angle $\theta = 0°$) minimum-energy configuration. This PES predicts a well depth of $D_e \approx 2420$ cm^{-1} at $R_e = 5.24a_0$. A second well in the linear HO−Kr configuration was estimated to have a well depth of 1900 cm^{-1} at a much shorter intermolecular distance of $4.16a_0$.

More recent ab initio RCCSD(T) calculations mapped out the electronically excited OH A $^2\Sigma^+$ + Kr PES for a fixed OH bond length.[6] This study revealed a significantly deeper potential well in the linear HO−Kr ($\theta = 180°$) configuration than on the prior empirical PES, with a substantially larger well depth of $D_e \approx 6079$ cm^{-1} at $R_e \approx 4.16a_0$. The HO−Kr minimum is separated from the linear OH−Kr configuration by a large barrier (greater than 1850 cm^{-1}). The properties of the OH−Kr well and its energy-level structure were in reasonable agreement with the prior work by Miller and co-workers, although some vibrational level reassignments were suggested. The study of Chadwick et al.[6] also included new experimental measurements of OH A $^2\Sigma^+$ + Kr rotationally inelastic scattering cross sections using Zeeman quantum beat spectroscopy. Both quantum-mechanical and quasiclassical trajectory scattering calculations were performed on the new OH A $^2\Sigma^+$ + Kr PES, yielding cross sections that were in good agreement with experiment.[6]

In this paper, we report the nascent OH X $^2\Pi$ product state distribution, including vibrational, rotational, and fine-structure propensities, as well as the cross sections for the quenching of OH A $^2\Sigma^+$ by Kr. Our measurements probe the regions of the OH A $^2\Sigma^+$ + Kr excited-state PES that allow for nonadiabatic coupling and efficient population transfer from the excited state to the OH X $^2\Pi$ + Kr ground-state surface. Complementary theoretical calculations show that the nonadiabatic coupling occurs in the HO−Kr well region, which has heretofore not been probed experimentally. The observed product state distributions are a measure of the forces on the OH radical as it passes through the strong nonadiabatic coupling region and subsequently separates from Kr on the ground-state surface.

EXPERIMENTAL METHODS

Two types of experiments were performed. The first, performed under jet expansion conditions (average collision energy of ∼0.025 eV) at the University of Pennsylvania, were used to determine lifetime and OH X $^2\Pi$ population data. The second set, performed under thermal conditions at 300 K at the University of Oxford, were used to determine thermally averaged collisional quenching cross sections. Since collisional quenching of OH A $^2\Sigma^+$ by many partners is known to be temperature-dependent, the two experiments cannot be compared quantitatively.

Lifetime and Population Measurements. The experimental methods for investigating the outcomes following collisional quenching of OH A $^2\Sigma^+$ by Kr were similar to those used previously at the University of Pennsylvania for other quenching partners.[13,14,16,17,19] Briefly, OH X $^2\Pi$ radicals were generated in the throat of a pulsed supersonic jet expansion by photolyzing nitric acid (98% fuming) at 193 nm. The nitric acid vapor was entrained in a 20% Kr/He gas mixture with a backing pressure of 80 psi. In the collision region of the expansion at a distance of $x/D = 5$, where D is the nozzle diameter, the OH radicals were excited on the $P_1(1)$ line of the A $^2\Sigma^+$−X $^2\Pi$ (0,0) transition with the UV pump laser operating at 308 nm. The pump-laser-induced fluorescence (LIF) was collected with a

dx.doi.org/10.1021/jp407035p | J. Phys. Chem. A 2013, 117, 13481−13490

photomultiplier tube (PMT) (ET Enterprises 9813Q) using a 308 nm bandpass filter. After a 100 ns delay, a spatially overlapped and counterpropagating UV laser intersected the expansion and probed the quenched OH X $^2\Pi$ products by means of various OH A−X transitions with vibrational (v''), rotational (N''), and fine-structure resolution. Probe LIF signals were collected using the same PMT but with different bandpass filters. The probe laser excitation and fluorescence collection schemes were the same as those used in prior experiments with N_2 as a collision partner.[17]

The LIF signals were processed with a digital storage oscilloscope (LeCroy WaveRunner 6050A) and transferred to a laboratory computer for further analysis. The waveform traces were fit to single-exponential decays to determine fluorescence lifetimes and integrated over a fixed gate to obtain intensities. The probe LIF intensities, recorded under saturated LIF conditions, were scaled relative to a reference line and converted to relative OH X $^2\Pi$ populations using the same analysis procedure as described previously.[13,14,16,17,19] The analysis procedure accounted for the lifetime and fluorescence quantum yield (Φ_f) of the emitting state as well as the filter transmission function.

An active background subtraction scheme[13,14,16,17,19] was used in data collection. Briefly, the pump laser (5 Hz) was operated at half the repetition rate of the probe laser (10 Hz). The background signal arising from the probe laser only was subtracted from the combined pump and probe laser-induced signal. This scheme enabled the desired signal arising from the combination of the pump and probe lasers to be distinguished from the background signals originating from the probe laser only.

Thermally Averaged Electronic Quenching Cross Sections. Absolute, thermally averaged cross sections for electronic quenching of OH A $^2\Sigma^+$ by Kr at 300 K were measured at the University of Oxford. The methods used were the same as described in previous studies[6] and so are summarized here only briefly.

OH X $^2\Pi$ was generated by the photolysis of hydrogen peroxide or nitric acid at 193 nm and excited to the A $^2\Sigma^+$ state on the (0,0) band with a pulsed dye laser after a delay of around 10 μs to allow the radicals to thermalize translationally. A photoelastic modulator (PEM) was used to switch the laser polarization direction either parallel or perpendicular to the detection axis on alternate shots. The resulting fluorescence from OH A $^2\Sigma^+$ was passed through a linear polarizer and detected by a PMT.

The fluorescence traces from the parallel ($I_{\parallel}$) and perpendicular ($I_{\perp}$) laser polarization directions with respect to the detection axis were fit using $I_{\parallel} + 2I_{\perp}$, which is sensitive only to the decay in population and independent of the decay in polarization. The data were fitted to a single-exponential function,

$$I = Ae^{-(k_f + k_Q[\mathrm{Kr}])t} \quad (1)$$

where k_f is the inverse of the fluorescence lifetime and k_Q is the quenching rate constant. By measurement of decays over a range of Kr pressures from ∼100 to ∼600 mTorr, k_Q was determined and converted into a thermally averaged quenching cross section using the expression $\sigma_Q = k_Q(T)/\langle v_{rel}\rangle$. Errors were taken as one standard deviation for comparison with the literature.[5]

In these unresolved measurements, rotational energy transfer (RET) does not directly contribute to the decay rate of the OH(A) emission. However, significant RET between rotational levels of OH(A) would scramble the initial-state selectivity of the electronic quenching measurements. For this reason, only the first ∼100 ns of the fluorescence decay was fitted to ensure that the measured electronic quenching rate constants were specific to a single N level. Detailed simulations and fits were performed as described in ref 36 to verify that this procedure yielded the correct initial-state-selected electronic quenching rate constants within the quoted errors in the measurements.

EXPERIMENTAL RESULTS

OH A $^2\Sigma^+$ Lifetimes. The OH radicals prepared in the lowest rovibrational level (v = 0, N = 0) of the excited A $^2\Sigma^+$ electronic state have a fluorescence lifetime of 400(15) ns in the collisional region of the supersonic expansion, which is significantly shorter than the radiative lifetime of ∼700 ns. Collisions with Kr in the 20% Kr/He carrier gas mixture are relatively efficient in quenching OH A $^2\Sigma^+$ (v = 0, N = 0); pure He carrier gas does not quench the fluorescence. With a 20% N_2/He carrier gas mixture at 80 psi under similar experimental conditions, the fluorescence lifetime (k_{tot}^{-1}) is approximately 320 ns. The fluorescence lifetimes measured for the each of the OH A $^2\Sigma^+$ (v = 0, N) and (v = 1, N) levels accessed by the probe laser are shown in Figure 1, with the values at each N averaged over spin−rotation components. These data were used in the analysis of OH X $^2\Pi$ populations. The experimentally measured total rate at each N (k_{tot}) is the sum of the collisional (k_{coll}), radiative (k_{rad}), and electronic predissociation (k_{PD}) rates. The radiative and electronic predissociation rates for OH A $^2\Sigma^+$ are tabulated in LIFBASE.[37] The pseudo-first-order collisional rates, k_{coll}, were readily extracted and are plotted in Figure 1.

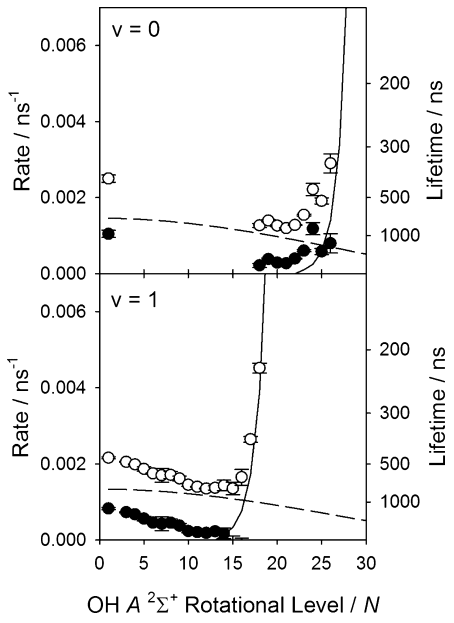

Figure 1. Experimentally determined OH A $^2\Sigma^+$ total decay rates (k_{tot}, ○) for v = 0 (top) and v = 1 (bottom) as functions of rotational level (N) in the collisional region of the supersonic expansion (average collision energy of ∼0.025 eV). The pseudo-first-order collisional rates (k_{coll}, ●) were derived from the radiative (k_{rad}, dashed line) and predissociative (k_{PD}, solid line) rates from ref 37.

In OH A $^2\Sigma^+$ (v = 0), the pseudo-first-order collisional rate is due solely to collisional quenching. The rate is largest for N = 0

dx.doi.org/10.1021/jp407035p | J. Phys. Chem. A 2013, 117, 13481−13490

and smaller for the high N levels examined in this work, remaining fairly constant from N = 18−22 but then increasing slightly at high N; the latter effect is similar to but less pronounced than that seen previously in collisions with N_2.[17] These highest N levels are above the energetic threshold to v = 1, possibly indicating a rotational (v = 0, high N) to vibrational (v = 1, low N) energy transfer process. In OH A $^2\Sigma^+$ (v = 1), the collisional rate is the sum of the collisional quenching and vibrational energy transfer rates, which cannot be decoupled in this experiment. The collisional rate decreases with increasing N. In the present experiments with Kr, the radiative rate at low N is larger than the collisional rate.

OH A $^2\Sigma^+$ Electronic Quenching Cross Sections. Absolute, thermally averaged electronic quenching cross sections at 300 K for OH A $^2\Sigma^+$ by Kr are presented in Figure 2, which is split into two panels for quenching from the F_1 (j = N + S) and F_2 (j = N − S) spin−rotation levels of OH A $^2\Sigma^+$. Figure 2 presents a much more extensive data set than that reported in our previous publication.[6] The thermally averaged cross sections are compared to the results of Hemming et al.[5] (it should be noted that the spin−rotation level employed was not specified in that work). The agreement with the literature is seen to be excellent and supports the smooth downward trend in σ_Q with N, with σ_Q falling to zero around N = 10. As the OH(A) radical rotates faster, fewer collisions are able to sample the conical intersection region in the HO(A)−Kr well and as a consequence are unable to undergo electronic quenching. Only a very small difference between the electronic quenching cross sections for the F_1 and F_2 spin−rotation levels was observed.

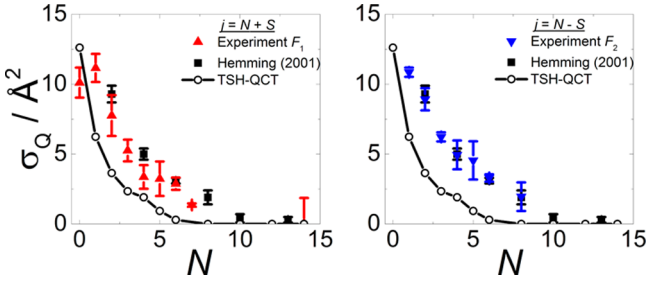

Figure 2. Electronic quenching cross sections for OH A $^2\Sigma^+$ (v = 0) with Kr under thermal conditions at 300 K. Left (red) F_1; right (blue) F_2; black squares, Hemming et al.[5] The open circles denote TSH-QCT closed-shell quenching cross sections. It should be noted that the spin−rotation level employed by Hemming et al. is not specified in their paper.

OH X $^2\Pi$ Product State Distribution. Relative populations were measured for over 40 distinct OH X $^2\Pi$ product quantum states. In some cases, individual OH X $^2\Pi$ levels could not be probed because of spectral congestion, the rapid onset of predissociation at high N (especially in v = 1), or a large OH X $^2\Pi$ background at low N'' (v'' = 0), preventing acceptable signal-to-noise ratios during the active background subtraction procedure. The population distribution is shown in Figures 3 and 4, plotted as a function of OH X $^2\Pi$ internal energy and rotational quantum number, respectively.

To aid in analysis of the population distribution, an arbitrary functional form was fit to the distribution after scaling of v'' = 1 to v'' = 0. A sum of two Fisher−Tippet functions was used here in order to capture the shape of the distribution.[38] The v'' = 0 and v'' = 1 distributions have similar shapes, exhibiting a peak at around 9 quanta of rotation, a slight dip in population, and then

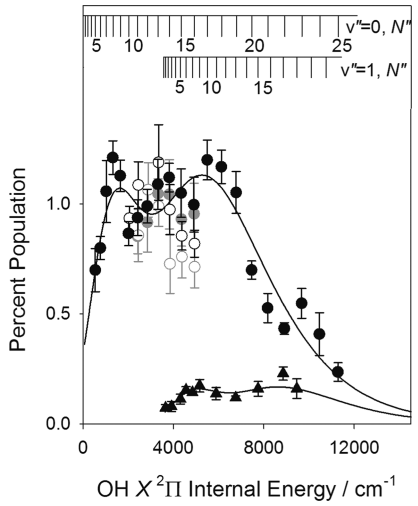

Figure 3. Nascent OH X $^2\Pi$ quantum state distribution observed following quenching of OH A $^2\Sigma^+$ (v = 0, N = 0) by Kr as a function of OH X $^2\Pi$ internal energy. Percent populations for v'' = 0 (circles) and v'' = 1 (triangles) are depicted. The F_1 and F_2 manifolds of the OH X$^2\Pi$ state are shown in solid and open symbols, respectively, with black and gray symbols representing the $\Pi(A')$ and $\Pi(A'')$ Λ doublets, respectively. The fit through the data is primarily used as a guide to the eye, as described in the text.

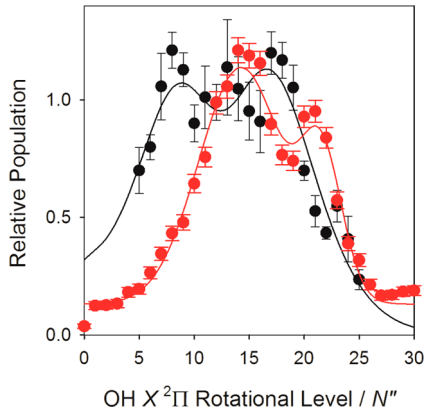

Figure 4. Nascent OH X $^2\Pi$ quantum state distribution observed following quenching of OH A $^2\Sigma^+$ (v = 0, N = 0) by Kr as a function of rotational level, N''. For simplification, the $\Pi(A')$ Λ doublet for v'' = 0 is depicted as an average of the F_1 and F_2 manifolds (black circles). The OH X $^2\Pi$ rotational distribution resulting from QCT surface-hopping calculations (red circles) was arbitrarily scaled to the peak of the experimental distribution. The same functional form was used to fit both sets of data and is primarily used as a guide to the eye, as described in the text.

a second peak at around 17 quanta of rotation. The distribution drops off at high and low N''. When the populations in specific product states for v'' = 0 and v'' = 1 were compared, a ratio of ∼7 times more population in v'' = 0 than in v'' = 1 was found.

In v'' = 0, all four spin−orbit (F_1 and F_2) and Λ-doublet [Π (A′) and Π (A″)] states were probed for N'' = 11−16. For a given Λ-doublet component, the populations in equivalent (same N'') F_1 and F_2 levels were found to be approximately the same within experimental uncertainty. The degree of electron alignment (DEA) is defined as $[P_{\Pi(A')} - P_{\Pi(A'')}]/[P_{\Pi(A')} + P_{\Pi(A'')}]$, which has limiting values of +1 and −1 associated with the unpaired electron being in the pπ orbital aligned in and out of the plane of molecular rotation, respectively. The DEA was

dx.doi.org/10.1021/jp407035p | J. Phys. Chem. A 2013, 117, 13481−13490

found to be 0.06(7), indicating little to no Λ-doublet propensity. This was tested again at a shortened pump−probe time delay (40 ns), and the same result was obtained within experimental uncertainty.

A branching fraction measurement was carried out following analogous studies with other quenching partners.[15−17,19] The amount of initially prepared OH A $^2\Sigma^+$ (v = 0, N = 0) was compared with four different OH X $^2\Pi$ product levels, two in v'' = 0 and two in v'' = 1. Approximately 1.1% of the quenched products were found in N'' = 13 and 14 of v'' = 0, 0.12% in N'' = 13 of v'' = 1, and 0.16% in N'' = 15 of v'' = 1. To determine the total branching to OH X $^2\Pi$ (v'' = 0, 1) products, the fit to the data was used to estimate the population in unobserved quantum states. Assuming a DEA of 0.06 and equal populations in the F_1 and F_2 states, approximately 95(7)% of the total quenched population can be identified in v'' = 0 [83(7)%] and v'' = 1 [12(1)%].

THEORETICAL METHODS AND RESULTS

Potential Energy Surfaces and Couplings. The ground X $^2\Pi$ and first excited A $^2\Sigma^+$ states of the OH molecule differ in the filling of the nonbonding $2p_\pi$ orbitals and the bonding 3σ orbital (formed from the bonding combination of the O $2p_\sigma$ and H 1s orbitals). The electronic configuration of the X state is $2p_\pi^3 3\sigma^2$, while that of the A state is $2p_\pi^4 3\sigma^1$. The A state lies 4.06 eV above the ground state.

The approach of the spherically symmetric Kr atom lifts the degeneracy of the $2p_\pi$ orbitals, splitting the Π state into a state that is symmetric (A′) with respect to reflection in the plane of the three atoms (which we take to be the yz plane), with electronic configuration $2p_{\pi x}^2 2p_{\pi y}^1 3\sigma^2$, and a state that is antisymmetric (A″), with electronic configuration $2p_{\pi x}^1 2p_{\pi y}^2 3\sigma^2$. We label these states $\Pi_{A'}$ and $\Pi_{A''}$, respectively. In nonlinear geometries, approach of the Kr can mix the A′ component of the X $^2\Pi$ state with the A $^2\Sigma^+$ state, in which the electronic wave function also has A′ reflection symmetry. We label this second A′ state as $\Sigma_{A'}$. This Π/Σ notation for the two diabatic states of A′ reflection symmetry follows earlier work on electronic quenching by Alexander and Corey[39] and Dagdigian et al.[40] For illustration, we show in Figure 5 contour plots of the OH 3σ (panel a) and $2p_{\pi y}$ (panel b) molecular orbitals discussed above, corresponding to the Kr−OH $\Sigma_{A'}$ and $\Pi_{A'}$ states, respectively. The $2p_{\pi x}$ molecular orbital (not shown) is similar to the $2p_{\pi y}$ orbital in panel b but perpendicular to the plane of the triatomic.

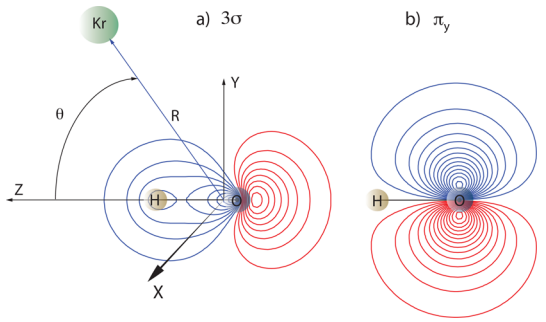

Figure 5. Visualization of the approach of the Kr atom (green sphere) to the OH (a) 3σ and (b) π_y orbitals with shapes depicted qualitatively. Both of the orbitals are symmetric (A′) with respect to reflection in the triatomic plane.

As mentioned before, last year Chadwick et al.[6] reported calculations of the Kr−OH (A $^2\Sigma^+$) PES that revealed a deep minimum for collinear Kr−OH approach. These authors characterized the single $\Sigma_{A'}$ PES at the coupled-cluster [RCCSD(T)] level and calculated rovibrational bound levels and cross sections for RET within the A $^2\Sigma^+$ state. The calculated RET cross sections obtained on the single PES surface slightly overestimated the experimental results, which suggested the presence of a collisional quenching pathway that was not included in the theoretical model. The ab initio PES of Chadwick et al.[6] was determined within a coupled-cluster method, which is single-reference in nature and cannot describe well the two PESs of A′ symmetry in the region where they cross. Here we show that the crossing between the $\Pi_{A'}$ and $\Sigma_{A'}$ Kr−OH PESs leads to significant nonradiative collisional quenching.

To determine the $\Pi_{A'}$ and $\Sigma_{A'}$ Kr−OH PESs, the coupling between these two diabatic states, and the PES for the single state of A″ reflection symmetry ($\Pi_{A''}$), we used the MOLPRO suite of ab initio codes. We maintained the OH distance at the value for isolated OH in the A state, r_e = 1.0121 Å.[41] We used an augmented correlation-consistent triple-ζ basis set, optimized for all-electron scalar relativistic calculations with Douglas−Kroll integrals (aug-cc-pvtz-DK).[42] Multiconfigurational Hartree−Fock (MCSCF) calculations were done, followed by multireference configuration-interaction calculations with inclusion of single and double excitations and addition of the Davidson correction (MRCISD+Q) to reduce the error associated with the lack of size consistency.

These calculations yielded three adiabatic PESs, two of A′ and one of A″ reflection symmetry, which we label 1A′, 2A′, and 1A″. Making use of the quasi-diabatization capability in MOLPRO, we then transformed (as defined in the next two equations) the 1A′ and 2A′ adiabatic states into the $\Pi_{A'}$ and $\Sigma_{A'}$ quasi-diabatic basis. The adiabatic and diabatic states of A′ reflection symmetry are related by a 2 × 2 orthogonal transformation as follows:

$$\begin{bmatrix} V_{1A'} & 0 \\ 0 & V_{2A'} \end{bmatrix} = \mathbf{C} \begin{bmatrix} V_{\Pi_{A'}} & V_{\Sigma\Pi} \\ V_{\Sigma\Pi} & V_{\Sigma_{A'}} \end{bmatrix} \mathbf{C}^{\mathrm{T}} \tag{2}$$

where

$$\mathbf{C} = \begin{bmatrix} \cos\gamma & \sin\gamma \\ -\sin\gamma & \cos\gamma \end{bmatrix} \tag{3}$$

Here, the mixing angle γ as well as the two diagonal and the off-diagonal diabatic PESs are functions of the three internal coordinates of the OH−Kr system. As expressed in eqs 2 and 3, the two adiabatic states represent an orthogonal admixture of the electronic configuration of the A state and the electronic configuration of the A′ component of the X state.

In the quasi-diabatization, the MCSCF orbitals are first rotated to maximize the overlap with a set of reference orbitals, taken here to be those for collinear KrOH at a large Kr−O distance, where the A and X states are well-separated in energy. The three diabatic PESs are then obtained by analysis of the CI coefficients in the basis of configurations built from the rotated orbitals. The third quasi-diabatic state, $\Pi_{A''}$, is unaffected by the adiabatic → quasi-diabatic transformation of the two A′ states and is identical to the 1A″ adiabatic state. At large OH−Kr distances, the two diabatic and adiabatic states of A′ reflection

dx.doi.org/10.1021/jp407035p | J. Phys. Chem. A 2013, 117, 13481−13490

symmetry become identical and correlate with the OH(X) + Kr and OH(A) + Kr asymptotes.

In the electronically adiabatic basis, the off-diagonal matrix elements of the derivative operator are responsible for the nonadiabatic coupling between the two states of A′ symmetry. It is easy to show from eqs 2 and 3 that this matrix element, the so-called nonadiabatic coupling matrix element (NACME), is equal to the derivative of the mixing angle, namely,

$$\langle 1A'|\frac{\partial}{\partial q}|2A'\rangle = \frac{\partial \gamma}{\partial q} \tag{4}$$

where q designates any of the three Jacobi coordinates. Equivalently, we can use the gradient operator to define a nonadiabatic coupling vector

$$\langle 1A'|\vec{\nabla}_q|2A'\rangle = \vec{\nabla}_q \gamma \tag{5}$$

The PESs were determined on a grid in Jacobi coordinates, R (ranging from 2.75 to 15 bohr) and θ (ranging from 0° to 180° in steps of 20° and including 90°). To obtain interaction energies, we subtracted the energy at a large separation between Kr and OH. The calculated interaction energies were not corrected for basis-set superposition error. Figure 6 shows radial cuts of the resultant adiabatic and diagonal diabatic PESs of A′ symmetry in nearly linear configurations. Figure 7 shows a surface plot of the two diabatic states, oriented to show clearly the small region of the crossing. This figure represents a 2D extension of Figure 6. Figure 8 displays a surface plot of the $V_{\Sigma\Pi}$ PES, which is the off-diagonal coupling in the diabatic basis.

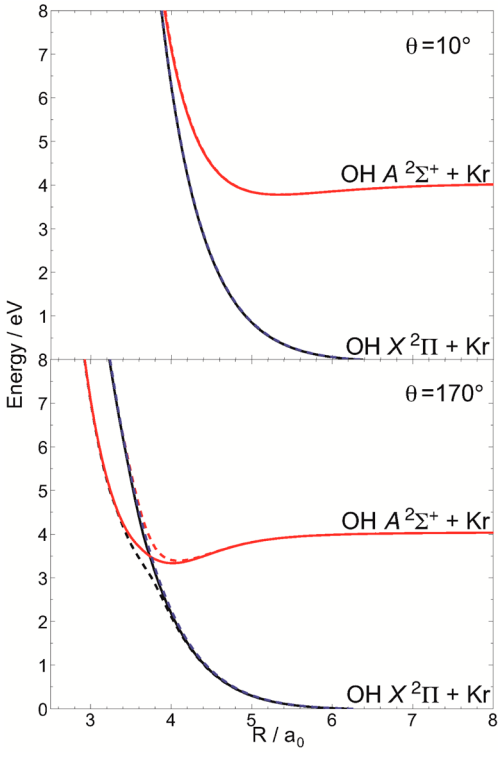

Figure 6. OH (X $^2\Pi$, A $^2\Sigma^+$) + Kr MRCISD+Q potential energy curves for the two states of A′ reflection symmetry, $\Pi_{A'}$ (solid black) and $\Sigma_{A'}$ (solid red), as functions of the OH−Kr center-of-mass distance for nearly collinear OH−Kr (top panel) and HO−Kr (bottom panel) orientations. The black and red dashed lines indicate the 1A′ and 2A′ electronically adiabatic potential curves, and the blue dashed line is the 1A″ adiabatic potential curve.

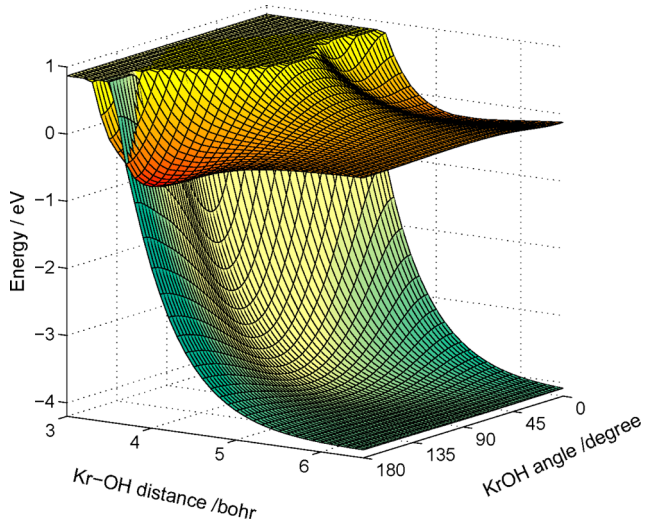

Figure 7. Surface plots relative to the OH A $^2\Sigma^+$ + Kr asymptote for the $\Pi_{A'}$ (green, lower surface) and $\Sigma_{A'}$ (orange, upper surface) diabatic states as functions of the OH to Kr center of mass distance (R, in bohr) and the angle of OH with respect to Kr (θ, in deg). The angle is defined in Figure 5, where 0° and 180° correspond to linear OH−Kr and linear HO−Kr, respectively.

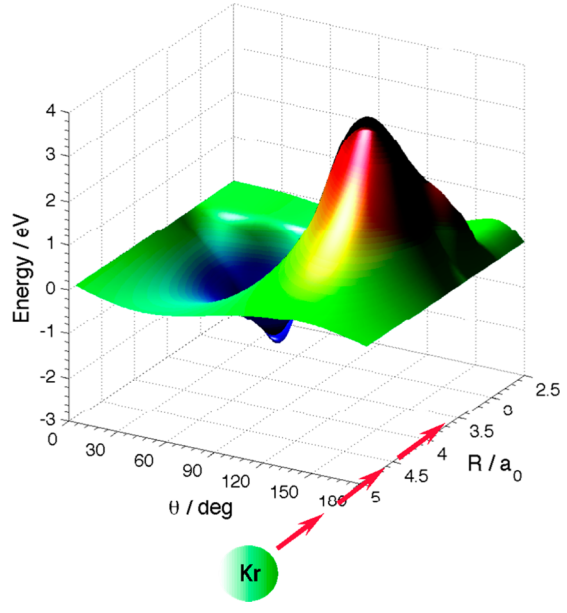

Figure 8. MRCISD+Q diabatic coupling $V_{\Sigma\Pi}$ PES. The coupling vanishes at the linear geometry and changes sign at a nearly perpendicular geometry.

In the Kr−OH linear geometry, the V_{Σ_A} PES is crossed by the repulsive wall of the V_{Π_A} PES at energies below the Kr + OH(A) asymptote, as shown in Figure 6 for θ = 170°. It is the presence of the deep, close-in Kr−OH(A) minimum that permits collisions at thermal and modestly hyperthermal energies to access this crossing. A crossing occurs in the other collinear geometry (Kr−HO), but it is at a much higher energy far above the Kr + OH(A) asymptote, as illustrated in Figure 6 for θ = 10°. The conical intersections in the two linear

dx.doi.org/10.1021/jp407035p | J. Phys. Chem. A 2013, 117, 13481−13490

geometries become avoided crossings in bent geometries, as shown in Figure 6.

This mixing of the two diabatic states provides a mechanism for electronic quenching of the OH A state in collisions with Kr. We observe in Figure 6 that this crossing is accessible for thermal or hyperthermal collisions only for nearly linear KrOH geometries (e.g., θ = 170° in Figure 6). The extent of this mixing is governed by the strength of the coupling between the $\Pi_{A'}$ and $\Sigma_{A'}$ diabats ($V_{\Sigma\Pi}$).

Trajectory Surface Hopping Calculations. The quasi-classical trajectory (QCT) method employed in this work was similar to that described in previous papers,[6,43] and only those details relevant to the present work are included here. The nonadiabatic classical calculations were carried out by the trajectory surface hopping (TSH) method[44] using the *fewest switches* algorithm proposed by Tully.[45] Trajectories were propagated classically on the electronically adiabatic 1A′ and 2A′ PESs. Each trajectory was started on the upper PES. In the QCT-TSH method, the kinetic coupling between these two states is the product of the NACMEs (eq 4) and the nuclear velocities. As shown in eq 4, the NACMEs are derivatives of the mixing angles, which can be evaluated (eqs 2 and 3) from the off-diagonal diabatic $V_{\Sigma\Pi}$ PES and the adiabatic potentials. The evolution of the electronic population in the two states of A′ reflection symmetry with the nuclear motion was controlled by integrating the time-dependent Liouville equation of the density matrix with a predictor−corrector Adams−Bashforth−Moulton algorithm simultaneously with the trajectory propagation.

Fast variations of the electronic populations can cause trajectories to jump from the current electronic state to any other of the same symmetry. We found that a time step of 0.05 fs was sufficiently small to ensure the conservation of the trace of the density matrix (i.e., the total electronic population) as well as the total energy of the system. Batches of 3×10^5 trajectories were run for each initial level at a collision energy of 39 meV. The initial distance between the incoming atom and the center of mass of the diatom was chosen to be 12 Å. The assignment of the final rotational level of the OH, N'', was carried out by equating the classical rotational angular momentum to $\hbar[N''(N''+1)]^{1/2}$. Real values of N'' were rounded to the nearest integer.

Also, in order to conserve the total energy of the system after a transition to another adiabatic PES, a kinetic energy correction was performed by rescaling the momentum of each nucleus in the direction of the nonadiabatic coupling vector (eq 5).[45,46] When the velocity component along the nonadiabatic coupling vector was not large enough to overcome the energy gap, the jump was forbidden. In the strong interaction region (the region of the Kr−OH well), trajectories were found to undergo several hops (usually one to four) between the 1A′ and 2A′ PESs. An even number of switches results in an inelastic transition on the original PES. An odd number of jumps gives rise to a quenched trajectory from the excited 2A′ state to the ground 1A′ state.

Figure 4 displays the comparison between the experimental and QCT-TSH rotational state distribution of the nascent OH X $^2\Pi$ formed by quenching from the lowest rotational level (N = 0) of the excited OH A $^2\Sigma^+$ state with Kr as the collision partner. At a fixed collision energy of E_{coll} = 39 meV, the total quenching cross section from the N = 0 level was found to be σ_Q(TOT) = 12.8 Å^2. As mentioned above, the theoretical prediction agrees with the experimental rotational distribution fairly well.

We also carried out QCT-TSH calculations for other initial OH A $^2\Sigma^+$ rotational levels (N = 0−14), always at E_{coll} = 39 meV. The QCT-TSH total quenching cross sections summed over the final levels (open circles) are compared with experiment in Figure 2. It should be noted that these calculations do not include the electron spin. Hence, identical results are displayed for both OH fine-structure levels in both panels of the figure.

The calculations successfully capture the correct order of magnitude for the quenching cross sections and the trend with increasing N, although the size of the quenching cross section is somewhat underestimated, especially with increasing OH rotation. The present TSH calculations consider only transitions between the upper and lower A′ states induced only by mixing of the two dominant electron occupancies of these states. Specifically not included is Coriolis coupling between the nominally Σ and Π states. This would provide an additional pathway for collisional quenching of the 2A′ state. Since the magnitude of the Coriolis coupling depends on the OH rotational quantum number, it would lead to a selective increase in quenching for the higher rotational levels. If this effect were sufficiently large, it would bring the theoretical results into better agreement with experiment.

DISCUSSION

Collisional electronic quenching of OH A $^2\Sigma^+$ by Kr results in OH X $^2\Pi$ products formed primarily in the lowest vibrational level with a substantial degree of rotational excitation and essentially no pπ orbital alignment (or Λ-doublet propensity). Branching fraction measurements for specific OH X $^2\Pi$ product states were used to scale the overall product state distribution, which then accounts for nearly all of the quenching events. These experimental observables can be understood in terms of the properties of the PESs, in particular the diabatic coupling and angular gradients in the vicinity of the avoided crossing.

The minimal vibrational excitation is consistent with the small change in OH bond length between the ground and excited electronic states (r_e = 0.9697 and 1.0121 Å, respectively). The degree of vibrational excitation (83% and 12% in v'' = 0 and 1, respectively) agrees well with the squares of the vibrational overlaps of OH A (v = 0) with OH X (v'' = 0) and OH X (v'' = 1) (the Franck−Condon factors), based on which we would predict a relative OH X $^2\Pi$ vibrational distribution of 90.5% in v'' = 0 and 9.2% in v'' = 1. Since quenching of OH A $^2\Sigma^+$ (v = 0) by Kr leads overwhelmingly to OH X (v'' = 0) products, the approximation of a frozen OH distance, made here in our theoretical simulations, should be justified.

The same quenching process results in significant rotational excitation, with an average rotational energy $\langle E_{rot}\rangle$ of 4400 cm^{-1} and average rotational quantum number $\langle N''\rangle$ of 14 in v'' = 0. The QCT calculations predict a similarly high degree of rotational excitation, with $\langle E_{rot}\rangle$ = 5300 cm^{-1} and $\langle N''\rangle$ = 18. The overall shape of the QCT product rotational distribution is quite similar to the experimental result, and the same fitting function (sum of two Fisher−Tippet functions) was used to guide the eye in Figure 4. On the basis of this fit, the QCT distribution peaks at ∼14 quanta of OH rotation, followed by a slight dip, and then has a secondary peak at ∼21 quanta of OH rotation. The physical origin of the slight dip could be the existence of different pathways from the region of nonadiabatic

dx.doi.org/10.1021/jp407035p | J. Phys. Chem. A 2013, 117, 13481−13490

coupling, resulting in the application of different torques to the OH radical; however, this has not been explored in depth. The significant rotational excitation seen here in our experimental and QCT theoretical studies is a characteristic feature in nonreactive quenching of OH A $^2\Sigma^+$ by many molecular collision partners.[13−17,19] Nevertheless, only $\sim^1/_8$ of the available energy appears as rotation.

Features of the OH + Kr PESs provide insight into the mechanism for quenching and the origin of the degree of rotational excitation seen in the OH X $^2\Pi$ product state distributions. As revealed by Figure 7, at low collision energies the crossing between the V_Σ and V_Π potentials is accessible only for nearly linear Kr−OH configurations ($\theta \geq 160°$). A barrier on the excited-state surface separates the OH−Kr and Kr−OH configurations and restricts access to the narrow Kr−OH well region where the ground and excited diabatic surfaces cross. The strong dependence of the quenching on the OH A $^2\Sigma^+$ orientation, specifically favoring the orientation in which the O side of OH points toward Kr, has been seen in theoretical studies involving several molecular partners, most notably the OH + H_2 and OH + N_2 systems.[17,22]

On the excited-state surface, an attractive interaction directs the approaching partners toward either the linear HO−Kr configuration (the global minimum) or the linear OH−Kr configuration (a local minimum). In the deeper HO−Kr well, a narrow angular region about linearity is intersected by the ground-state surface at small R. The collision partners that access this narrow region are funneled down to the ground-state surface, where they experience a steep angular gradient away from the linear geometry. The strong torque resulting from this gradient results in significant rotational excitation of the OH X $^2\Pi$ products. Similar angular gradients on the potential surfaces have been identified previously in the OH + H_2 system and qualitatively linked to the degree of rotational excitation of the OH products.[11,13−20,27−29] On the other hand, the region of coupling between the ground and excited states is limited to nearly linear geometry (Figure 7), which sets a limit on the amount of rotational excitation. This would explain why only $^1/_8$ of the total available energy appears as OH rotation.

The coupling between the surfaces also plays an important role in the quenching events. The size of the off-diagonal coupling in the quasi-diabatic basis, shown in Figure 8, illustrates the strength of the mixing between the ground and excited A′ states. The coupling vanishes at the linear geometry, increases to a maximum near 120° at 3.1−3.2a_0, decreases in magnitude, and then changes sign at a nearly perpendicular geometry. The region of the strongest coupling is not energetically accessible. Nevertheless, coupling occurs throughout the crossing region in the HO−Kr well region with greater strength for increasingly bent configurations, thereby favoring these geometries in quenching events.

The surface-hopping QCT calculations presented here included only two PESs, the ground and excited A′ states. The agreement with the experimental quenching cross sections is reasonable, but the theory underestimates somewhat the true extent of the electronic quenching. It is possible that expanding the theoretical treatment to include the lowest A″ surface would increase the efficiency of quenching, leading to better agreement with experiment. In particular, the overall KrOH rotational motion should couple the excited $\Sigma_{A'}$ PES to the $\Pi_{A''}$ PES. Experimentally, the quenched OH products are distributed equally over the two Λ-doublet components of each rotational level, which differs from the results of previous studies with H_2 and N_2 collision partners, where a strong Π(A′) Λ-doublet preference was observed. The Λ-doublet propensity arising from quenching has not yet been examined theoretically. This suggests that an accurate model of the distribution of the OH(X) products among the fine-structure and Λ-doublet multiplets will require inclusion of both the $\Pi_{A'}$ and $\Pi_{A''}$ PESs.

■ CONCLUSIONS

Experiment reveals that OH A $^2\Sigma^+$ is efficiently quenched by collisions with Kr, leading to OH X $^2\Pi$ products in $v'' = 0$ and to a much lesser extent in $v'' = 1$. The minimal degree of vibrational excitation is consistent with the small difference in OH bond length in its ground and excited states, with nearly diagonal Franck−Condon overlap. The quenched products exhibit a significant degree of rotational excitation. This is well-predicted by quasiclassical trajectory calculations based on ab initio PESs.

We interpret the quenching in terms of crossings between these PESs. The calculated PESs associated with the two electronic states of A′ reflection symmetry cross in the linear KrOH geometry but undergo strong coupling as the triatomic system bends. This coupling gives rise to efficient population transfer from OH A $^2\Sigma^+$ ($v = 0$, $N = 0$) to OH X $^2\Pi$ (v'', N'') products. The crossing region is accessible at thermal or hyperthermal energies because of the deep well in the OH A $^2\Sigma^+$ + Kr PES. This well is shallower for the interaction of OH with the lighter noble gases. Thus, for interactions with the lighter noble gases, the crossing between the A and X states is inaccessible,[47] and the efficiency of electronic quenching is much lower.

Classical-trajectory surface-hopping calculations that included the coupling between the two A′ electronic states were able to account qualitatively for the electronic quenching cross sections and OH X $^2\Pi$ level populations observed experimentally. However, a careful comparison with experiment suggested that couplings to the lowest A″ PES might be important. Similar quantum simulations of the electronic quenching are in progress, the results of which will be presented elsewhere.

■ AUTHOR INFORMATION

Corresponding Author

*E-mail: milester@sas.upenn.edu.

Notes

The authors declare no competing financial interest.

■ ACKNOWLEDGMENTS

The research at the University of Pennsylvania was supported by the Office of Basic Energy Sciences of the U.S. Department of Energy (DE-FG02-87ER13792). M.H.A. and P.J.D. acknowledge the support of the National Science Foundation through Grant CHE-1213332. F.J.A. acknowledges financial support by the Spanish Ministry of Education and Science under Grants CTQ2008-02578/BQU, CSD2009-00038, and CTQ2012-37404-C02. M.B. thanks the EPSRC (U.K.) for Programme Grant EP/G00224X/1, which funded part of this research.

■ REFERENCES

(1) Crosley, D. R. Laser Fluorescence Detection of Atmospheric Hydroxyl Radicals. *Adv. Ser. Phys. Chem.* **1995**, *3*, 256−317.

(2) Creasey, D. J.; Heard, D. E.; Pilling, M. J.; Whitaker, B. J.; Berzins, M.; Fairlie, R. Visualization of a Supersonic Free-Jet Expansion Using

Laser-Induced Fluorescence Spectroscopy. Application to the Measurement of Rate Constants at Ultralow Temperatures. *Appl. Phys. B: Lasers Opt.* **1997**, *65*, 375−391.
(3) Heard, D. E.; Henderson, D. A. Quenching of OH(A $^2\Sigma^+$, $v' = 0$) by Several Collision Partners between 200 and 344 K. Cross-Section Measurements and Model Comparisons. *Phys. Chem. Chem. Phys.* **2000**, *2*, 67−72.
(4) Hemming, B. L.; Crosley, D. R. Rotational-Level Dependence of OH A $^2\Sigma^+$ Quenching at 242 and 196 K. *J. Phys. Chem. A* **2002**, *106*, 8992−8995.
(5) Hemming, B. L.; Crosley, D. R.; Harrington, J. E.; Sick, V. Collisional Quenching of High Rotational Levels in A $^2\Sigma^+$ OH. *J. Chem. Phys.* **2001**, *115*, 3099−3104.
(6) Chadwick, H.; Brouard, M.; Chang, Y. P.; Eyles, C. J.; Perkins, T.; Seamons, S. A.; Kłos, J.; Alexander, M. H.; Aoiz, F. J. A New Potential Energy Surface for OH(A $^2\Sigma^+$)−Kr: The van der Waals Complex and Inelastic Scattering. *J. Chem. Phys.* **2012**, *137*, No. 154305.
(7) Hogan, P.; Davis, D. D. Electronic Quenching and Vibrational Relaxation of the OH(A $^2\Sigma^+$, $v' = 1$) State. *J. Chem. Phys.* **1975**, *62*, 4574−4576.
(8) Hogan, P.; Davis, D. D. Comments on "Electronic Quenching and Vibrational Relaxation of the OH(A $^2\Sigma^+$, $v' = 1$) State". *J. Chem. Phys.* **1976**, *64*, 3901.
(9) Lengel, R. K.; Crosley, D. R. Comment on "Electronic Quenching and Vibrational Relaxation of the OH(A $^2\Sigma^+$, $v' = 1$) State". *J. Chem. Phys.* **1976**, *64*, 3900−3901.
(10) Wysong, I. J.; Jeffries, J. B.; Crosley, D. R. Quenching of A $^2\Sigma^+$ OH at 300 K by Several Colliders. *J. Chem. Phys.* **1990**, *92*, 5218−5222.
(11) Ortiz-Suárez, M.; Witinski, M. F.; Davis, H. F. Reactive Quenching of OH(A $^2\Sigma^+$) by D_2 Studied Using Crossed Molecular Beams. *J. Chem. Phys.* **2006**, *124*, No. 201106.
(12) Hancock, G. Personal communication.
(13) Cleary, P. A.; Dempsey, L. P.; Murray, C.; Lester, M. I.; Kłos, J.; Alexander, M. H. Electronic Quenching of OH A $^2\Sigma^+$ Radicals in Single Collision Events with Molecular Hydrogen: Quantum State Distribution of the OH X $^2\Pi$ Products. *J. Chem. Phys.* **2007**, *126*, No. 204316.
(14) Dempsey, L. P.; Murray, C.; Cleary, P. A.; Lester, M. I. Electronic Quenching of OH A $^2\Sigma^+$ Radicals in Single Collision Events with H_2 and D_2: A Comprehensive Quantum State Distribution of the OH X $^2\Pi$ Products. *Phys. Chem. Chem. Phys.* **2008**, *10*, 1424−1432.
(15) Dempsey, L. P.; Murray, C.; Lester, M. I. Product Branching between Reactive and Non-Reactive Pathways in the Collisional Quenching of OH A $^2\Sigma^+$ Radicals by H_2. *J. Chem. Phys.* **2007**, *127*, No. 151101.
(16) Dempsey, L. P.; Sechler, T. D.; Murray, C.; Lester, M. I. Quantum State Distribution of the OH X $^2\Pi$ Products from Collisional Quenching of OH A $^2\Sigma^+$ by O_2 and CO_2. *J. Phys. Chem. A* **2009**, *113*, 6851−6858.
(17) Dempsey, L. P.; Sechler, T. D.; Murray, C.; Lester, M. I.; Matsika, S. State-Resolved Distribution of OH X $^2\Pi$ Products Arising from Electronic Quenching of OH A $^2\Sigma^+$ by N_2. *J. Chem. Phys.* **2009**, *130*, No. 104307.
(18) Lehman, J. H.; Bertrand, J. L.; Stephenson, T. A.; Lester, M. I. Reactive Quenching of OD A $^2\Sigma^+$ by H_2: Translational Energy Distributions for H- and D-Atom Product Channels. *J. Chem. Phys.* **2011**, *135*, No. 144303.
(19) Lehman, J. H.; Dempsey, L. P.; Lester, M. I.; Fu, B.; Kamarchik, E.; Bowman, J. M. Collisional Quenching of OD A $^2\Sigma^+$ by H_2: Experimental and Theoretical studies of the State-Resolved OD X $^2\Pi$ Product Distribution and Branching Fraction. *J. Chem. Phys.* **2010**, *133*, No. 164307.
(20) Lehman, J. H.; Lester, M. I.; Yarkony, D. R. Reactive Quenching of OH A $^2\Sigma^+$ by O_2 and CO: Experimental and Nonadiabatic Theoretical Studies of H- and O-Atom Product Channels. *J. Chem. Phys.* **2012**, *137*, No. 094312.
(21) Alexander, M. H.; Andresen, P.; Bacis, R.; Bersohn, R.; Comes, F. J.; Dagdigian, P. J.; Dixon, R. N.; Field, R. W.; Flynn, G. W.; Gericke, K.-H.; et al. A Nomenclature for Λ-Doublet Levels in Rotating Linear Molecules. *J. Chem. Phys.* **1988**, *89*, 1749−1753.
(22) Hoffman, B. C.; Yarkony, D. R. The Role of Conical Intersections in the Nonadiabatic Quenching of OH(A $^2\Sigma^+$) by Molecular Hydrogen. *J. Chem. Phys.* **2000**, *113*, 10091−10099.
(23) Lester, M. I.; Loomis, R. A.; Schwartz, R. L.; Walch, S. P. Electronic Quenching of OH A $^2\Sigma^+$ ($v' = 0$, 1) in Complexes with Hydrogen and Nitrogen. *J. Phys. Chem. A* **1997**, *101*, 9195−9206.
(24) Yarkony, D. R. Current Issues in Nonadiabatic Chemistry. *J. Phys. Chem.* **1996**, *100*, 18612−18628.
(25) Yarkony, D. R. Substituent Effects and the Noncrossing Rule: The Importance of Reduced Symmetry Subspaces. I. The Quenching of OH(A $^2\Sigma^+$) by H_2. *J. Chem. Phys.* **1999**, *111*, 6661−6664.
(26) Miller, S. M.; Clary, D. C.; Kliesch, A.; Werner, H. J. Rotationally Inelastic and Bound State Dynamics of H_2−OH(X $^2\Pi$). *Mol. Phys.* **1994**, *83*, 405−428.
(27) Bowman, J. M.; Czakó, G.; Fu, B. High-Dimensional ab Initio Potential Energy Surfaces for Reaction Dynamics Calculations. *Phys. Chem. Chem. Phys.* **2011**, *13*, 8094−8111.
(28) Fu, B.; Kamarchik, E.; Bowman, J. M. Quasiclassical Trajectory Study of the Postquenching Dynamics of OH A $^2\Sigma^+$ by H_2/D_2 on a Global Potential Energy Surface. *J. Chem. Phys.* **2010**, *133*, No. 164306.
(29) Kamarchik, E.; Fu, B. N.; Bowman, J. M. Communication: Classical Trajectory Study of the Postquenching Dynamics of OH A $^2\Sigma^+$ by H_2 Initiated at Conical Intersections. *J. Chem. Phys.* **2010**, *132*, No. 091102.
(30) Zhang, P. Y.; Lu, R. F.; Chu, T. S.; Han, K. L. Nonadiabatic Quantum Reactive Scattering of the OH(A $^2\Sigma^+$) + D_2. *J. Chem. Phys.* **2010**, *133*, No. 174316.
(31) Zhang, P.-Y.; Lu, R.-F.; Chu, T.-S.; Han, K.-L. Quenching of OH(A $^2\Sigma^+$) by H_2 through Conical Intersections: Highly Excited Products in Nonreactive Channel. *J. Phys. Chem. A* **2010**, *114*, 6565−6568.
(32) Carter, C. C.; Lee, H. S.; McCoy, A. B.; Miller, T. A. The Structure of Floppy Molecules: the Rg·XH/D (Rg = Ar, Ne, and Kr, X = O or S) Family of Complexes. *J. Mol. Struct.* **2000**, *525*, 1−45.
(33) Carter, C. C.; Miller, T. A.; Lee, H. S.; Korambath, P. P.; McCoy, A. B.; Hayes, E. F. High Resolution Electronic Spectroscopy of Kr·OH/D and an Empirical Potential Energy Surface. *J. Chem. Phys.* **1999**, *110*, 1508−1520.
(34) Fei, S. L.; Zheng, X. N.; Heaven, M. C. Electronic Spectroscopy and Vibrational Predissociation Dynamics of OH−Kr and OD−Kr. *J. Chem. Phys.* **1992**, *97*, 1655−1663.
(35) Lemire, G. W.; Sausa, R. C. Detection and Spectroscopic Studies of Gas-Phase OH−Kr by Laser-Induced Fluorescence. *J. Phys. Chem.* **1992**, *96*, 4821−4824.
(36) Brouard, M.; Bryant, A.; Chang, Y.-P.; Cireasa, R.; Eyles, C. J.; Green, A. M.; Marinakis, S.; Aoiz, F. J.; Kłos, J. Collisional Depolarization of OH(A) with Ar: Experiment and Theory. *J. Chem. Phys.* **2009**, *130*, No. 044306.
(37) Luque, J.; Crosley, D. R. *LIFBASE: Database and Spectral Simulation Program*, version 1.6; SRI Report MP 99-009; SRI International: Menlo Park, CA, 1999.
(38) *Handbook of Mathematical Functions with Formulas, Graphs and Mathematical Tables*; Abramowitz, M.; Stegun, I., Eds.; Dover Publications: New York, 1972.
(39) Alexander, M. H.; Corey, G. C. Collision-Induced Transitions between $^2\Pi$ and $^2\Sigma$ States of Diatomic Molecules: Quantum Theory and Collisional Propensity Rules. *J. Chem. Phys.* **1986**, *84*, 100−113.
(40) Dagdigian, P. J.; Patel-Misra, D.; Berning, A.; Werner, H.-J.; Alexander, M. H. A Joint Experimental and Theoretical study of A $^2\Pi$−X $^2\Sigma^+$ Electronic Energy Transfer in the CN Molecule Induced by Collisions with He. *J. Chem. Phys.* **1993**, *98*, 8580−8592.
(41) Huber, K. P.; Herzberg, G. *Molecular Spectra and Molecular Structure. IV. Constants of Diatomic Molecules*; Van Nostrand Reinhold: New York, 1979.
(42) Wilson, A. K.; Woon, D. E.; Peterson, K. A.; Dunning, T. H., Jr. Gaussian Basis Sets for Use in Correlated Molecular Calculations. IX.

The Atoms Gallium through Krypton. *J. Chem. Phys.* **1999**, *110*, 7667−7676.
(43) Aoiz, F. J.; Brouard, M.; Eyles, C. J.; Kłos, J.; de Miranda, M. P. The Collisional Depolarization of $^{2S+1}\Sigma$ Radicals by Closed Shell Atoms: Theory and Application to OH(A $^{2}\Sigma^{+}$) + Ar. *J. Chem. Phys.* **2009**, *130*, No. 044305.
(44) Tully, J. C.; Preston, R. K. Trajectory Surface Hopping Approach to Nonadiabatic Molecular Collisions: The Reaction of H^{+} with D_2. *J. Chem. Phys.* **1971**, *55*, 562−572.
(45) Tully, J. C. Molecular Dynamics with Electronic Transitions. *J. Chem. Phys.* **1990**, *93*, 1061−1071.
(46) Fabiano, E.; Keal, T. W.; Thiel, W. Implementation of Surface Hopping Molecular Dynamics using Semiempirical Methods. *Chem. Phys.* **2008**, *349*, 334−347.
(47) Kłos, J.; Alexander, M. H.; Dagdigian, P. J. Work in progress.